

Robustness of type-II Dirac cones in biphenylene-based structures

L. L. Lage,¹ O. Arroyo-Gascón,^{2,3} Leonor Chico,³ and A. Latgé¹

¹*Instituto de Física, Universidade Federal Fluminense,
Niterói, Av. Litorânea sn 24210-340, RJ-Brazil*

²*Instituto de Ciencia de Materiales de Madrid, Consejo Superior de Investigaciones Científicas,
C/ Sor Juana Inés de la Cruz 3, 28049 Madrid, Spain*

³*GISC, Departamento de Física de Materiales, Facultad de Ciencias Físicas,
Universidad Complutense de Madrid, E-28040 Madrid, Spain*

(Dated: March 29, 2024)

The electronic properties of one- and two-dimensional biphenylene-based systems, such as nanoribbons and bilayers, are studied within a unified approach. Besides the bilayer with direct (AA) stacking, we present two additional symmetric stackings for bilayer biphenylene that we denote by AB, by analogy with bilayer graphene, and AX, which can be derived by a small translation (slip) from the AA bilayer, with distinct band structures. We combine first-principles calculations with a tight-binding model to provide a realistic effective description of these structures. Our approach provides a global framework to characterize and analyze the robustness of the type-II Dirac cone within these structures, captures the variations caused by different stackings, and highlights important symmetries inherent in the biphenylene nanoribbon Dirac cones and edge states.

I. INTRODUCTION

The discovery of graphene by mechanical exfoliation [1] and the uncovering of the relation between its unique geometry and peculiar properties have inspired a great effort in the exploration of new two-dimensional (2D) materials [2, 3]. The stacking of 2D crystals, the so-called van der Waals heterostructures, produces novel materials with properties that can be tuned by the appropriate choice of components [4]. Although this approach has provided a plethora of 2D crystals with disparate properties, from insulators to superconductors [5–7], carbon-derived 2D materials stand out, since carbon is the element of choice for its abundance and the possibility of integration with graphene in hybrid systems [8].

Carbon-based 2D crystals, particularly those based in hexagonal (benzene) rings, have attracted much interest, such as monolayer [9, 10] and bilayer [11, 12] graphyne systems, and its variations such as graphydyne [13], obtained by the insertion of *sp* acetylenic bonds within the carbon connections. Other carbon allotropes without hexagonal carbon rings have been theoretically proposed, such as pentaheptite [14], completely composed of pentagons and heptagons; or a semiconducting planar sheet formed by 4- and 8-atom carbon rings [15], and even a buckled 2D material made of distorted pentagons, known as pentagraphene [16, 17]. These two latter examples have the interest of being semiconductor planar forms of carbon which could complement graphene. Additionally, structures combining hexagonal and other *n*-carbon rings have been also proposed [18, 19]. Among them, biphenylene stands out due to its recent experimental synthesis via the dehydrofluorination fusion of benzenoid polyphenylene chains [20].

This planar *sp*² carbon network structure was proposed long ago [21]. It exhibits an intricate geometry, comprising 4-, 6- and 8-folded rings. Electronic stability of biphenylene systems was also studied before its syn-

thesis with first-principles calculations, including ribbons and tubes of different widths and morphologies [22].

After its experimental discovery, many works have explored the physical and chemical properties of biphenylene [23–26]. Density-functional theory (DFT) calculations identified a type-II Dirac cone with metallic character which could be useful for valleytronics related to the existence of two bands with the same sign of the carrier velocity [27–29]. However, a band gap can be achieved by applying strain or doping the lattice [30, 31]. Another way of producing a band gap is by doping with fluorine atoms; this technique can be also applied to tune the Dirac cone and change its character [32].

Further studies reveal that biphenylene may have properties of practical interest, such as being an anti-corrosion coating material with exceptional oxygen atom adsorption and reasonable hydrophobicity [33], or thermoelectric applications in the 2D system [34] and in nanoribbons [35, 36]. Theoretical results predict a semiconductor behavior for the armchair nanoribbons for small sizes (< 2 nm), and metallic for both, zigzag and larger armchair ribbons [20, 22].

Simple tight-binding models of monolayer biphenylene including only nearest-neighbor interactions predict a type-III Dirac cone with a sharp flat band that are at variance with those obtained by first-principles calculations. More recently, the topological properties of biphenylene were studied by means of a simple tight-binding model, which allowed to tune topological phase transitions by varying the electron hoppings and explore the higher-order topological properties of this material [37].

Regarding bilayer systems, the AA stacking in 2D biphenylene has been modeled within a DFT approach, predicting a stable configuration with enhanced elastic characteristics compared to its monolayer counterpart [38], but to the best of our knowledge, no other stackings have been considered so far.

Motivated by these works, we study another symmetric bilayer configurations, obtained by small displacements of one of the layers and with minimal translational unit cells. We also explore biphenylene nanoribbons, providing a tight-binding parametrization valid for these bilayers with symmetric stackings as well as for nanoribbons. We analyze the changes in the Dirac cones, showing the modifications produced by the interlayer interaction and by the size and symmetry effects related to the nanoribbons, such as an anticrossing that results in a gap opening in the Dirac cone, that is explained by the symmetry of the wavefunctions in such confined systems. We expect that our tight-binding model will be of interest for further explorations of complex carbon-based materials with hybrid geometric structures, providing a starting point for the modeling of more complex systems and properties.

II. SYSTEMS AND METHODS

In order to describe all the biphenylene structures, we start by performing a DFT relaxation of the geometries. With the relaxed coordinates, we perform a general tight-binding parametrization intended to be valid for all structures, i.e., not calculation-dependent, applicable for the monolayer, and also to nanoribbons and bilayers.

A. Geometry of monolayer biphenylene

Differently from graphene, monolayer biphenylene belongs to the $Pmmm$ group. It is described by a rectangular unit cell of orthogonal lattice vectors \vec{a}_1 and \vec{a}_2 , of unequal lengths $a_1 \neq a_2$, with a six-atom basis, as depicted in Fig. 1 (a). Note that the hexagon is not regular, and neighboring atoms are at two different distances, d_1 and d_2 . Repeating this pattern, the octagons and 4-atom rings show up, so four different distances between atoms are required. The first Brillouin zone, also rectangular, is depicted therein, with the four high-symmetry points labeled, namely, $\Gamma = (0, 0)$, $X = (\frac{\pi}{a_1}, 0)$, $Y = (0, \frac{\pi}{a_2})$, and $S = (\frac{\pi}{a_1}, \frac{\pi}{a_2})$.

B. Geometries of bilayers with symmetric stackings

The geometric stackings for bilayer biphenylene defined as AA, AB, and AX are depicted in Fig. 1(b). Bilayer AA is the trivial, direct stacking, obtained by placing two biphenylene layers one on top of the other. The AB stacking is obtained by starting from an AA stacking and displacing one of the layers a distance d_2 along the \vec{a}_2 direction. We chose this denomination because one atom belonging to a hexagon of the upper layer is at the center of the hexagon of the bottom layer, thus resembling the AB stacking of bilayer graphene. Finally, the AX bilayer is obtained by starting from the AA configuration and displacing one layer by a distance d_3 along the \vec{a}_1

direction; it resembles the so-called slip stacking visible in graphene moiré patterns [39, 40]. In all these cases the unit cell has 12 atoms, twice than that of the monolayer; the ideal (unrelaxed) lattice vectors are initially chosen to be the same as for the monolayer, and change after relaxation, as expected. The interlayer distance is close to that of graphene, and we obtained slightly different values after relaxation, as it will be discussed later.

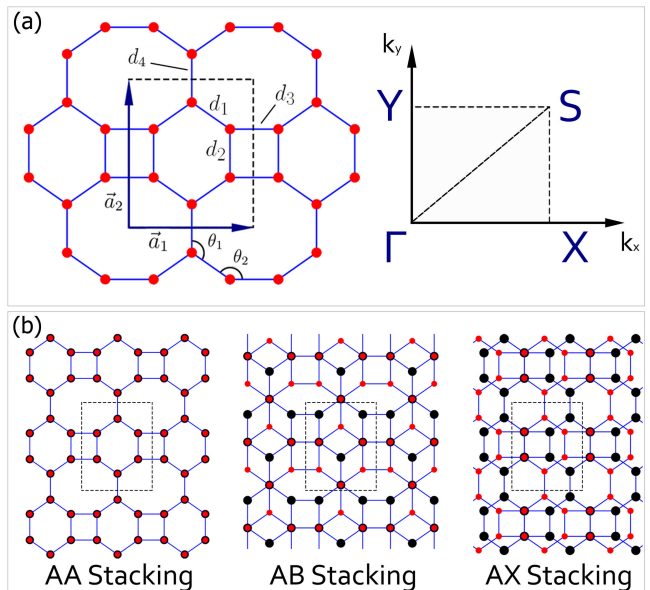


FIG. 1. (a) Left panel: 2D biphenylene lattice with primitive vectors \vec{a}_1 and \vec{a}_2 along the x and y direction, respectively. Right panel: first Brillouin zone of biphenylene with special symmetry lines and points. (b) Schematic depiction of the three bilayer stackings studied in this work.

C. DFT calculations

We have used the SIESTA first-principles code [41, 42] to perform electronic structure calculations, employing the generalized gradient approximation (GGA) and the Perdew–Burke–Ernzerhof (PBE) exchange–correlation functional [43]. This is our functional of choice for the monolayer system. For the bilayer geometries, additional van der Waals functionals following Dion et al. [44] with different improvements, namely DRSSL (equivalent to vdW-DF) [45] and LMKLL (equivalent to vdW-DF2) [46] flavors, were used. For all calculations, a double- ζ singly-polarized basis set was employed. The reciprocal space was mapped by means of a $8 \times 8 \times 1$ Monkhorst-Pack grid for all systems. All structures were relaxed until the forces were below 0.01 eV/Å.

D. Tight-binding approach

Our goal with the tight-binding approach is to provide a unified description of all biphenylene structures, rather than providing a specific parametrization tuned for each specific case. Since we focus on the bands around the Fermi energy, a single p_z orbital tight-binding (TB) Hamiltonian is used to describe the bilayer and monolayer systems, given by

$$H = \sum_{i,a} \varepsilon_i^a c_i^{\dagger a} c_i^a + \sum_{i,j}^a t_{ij}^a c_i^{\dagger a} c_j^a + \sum_{i,j}^a t_{ij}^{\perp ab} c_i^{\dagger a} c_j^b + h.c. \quad (1)$$

where ε_i^a is the onsite energy for each atom located at site i in layer a , and the operator $c_i^{\dagger a}$ (c_i^a) creates (annihilates) an electron on site i and layer a . The second term describes the intralayer couplings, t_{ij}^a being the corresponding hopping energies within layer a . Obviously for monolayers $a = 1$, and for bilayers we consider two values $a(b) = 1, 2$, as well as the interlayer interactions, given by the last term ($a \neq b$) and denoted as $t_{ij}^{\perp ab}$. They depend on the stacking configuration between top and bottom biphenylene layers.

To find a suitable hopping parametrization we have considered an intralayer hopping energy described by a decaying exponential function [40], $t_{ij}^a = t_1 e^{-\beta(\frac{r_{ij}}{d_1} - 1)}$, with r_{ij} being the distance between i, j lattice sites, t_1 the hopping related to the first nearest-neighbor distance d_1 , and β a fitting parameter that controls the range of the interaction. As the ratio r_{ij}/d_1 is always larger than one beyond the first nearest-neighbors, small β values allows to increase the number of neighbors with non-negligible hoppings in the description.

For the interlayer connection we have also considered a decaying exponential function for the hopping energies given by $t_{ij}^{\perp ab} = t_0 e^{-\alpha(r_{ij} - d_{\perp})}$, with d_{\perp} being the interlayer distance, t_0 is the direct stacking hopping value, i.e., when the atoms are exactly one above the other, and α modulates the strength of the interlayer hopping with increasing distance.

III. TWO-DIMENSIONAL BIPHENYLENE SYSTEMS

A. Monolayer biphenylene

The relaxed geometries obtained by DFT (PBE-GGA) for the monolayer are the following: the lengths of the lattice vectors are $a_1 = 3.815 \text{ \AA}$ and $a_2 = 4.544 \text{ \AA}$, with octagon angles $\theta_1 = 125^\circ$ and $\theta_2 = 145^\circ$. The four distances between atoms with primary covalent bonds, defined in Fig. 1 (a), are given by $d_1=1.42 \text{ \AA}$, $d_2=1.44 \text{ \AA}$, $d_3=1.50 \text{ \AA}$, and $d_4=1.47 \text{ \AA}$. The basis vectors can

be written as $\vec{a}_1 = (2d_1 \sin(\pi - \theta_2) + d_3, 0)$ and $\vec{a}_2 = 2(0, d_1 \cos(\pi - \theta_2) + d_2)$.

We present in Fig. 2(a) a comparison between DFT PBE-GGA (dotted blue curves) and the fitted tight-binding (full orange lines) electronic band calculations. The agreement is very good for the fitting parameters shown in Table I, specially in the energy range close to the Fermi level. The density of states (DOS) obtained from the TB approach is displayed at the right of the electronic bands. The peculiar type-II Dirac cone appearing in the middle of the $Y - \Gamma$ path can be clearly seen in Fig. 2(a); it is correctly described by the TB model. A 2D plot of the band structure is depicted in Fig. 2(b) where the type-II cone is highlighted in orange.

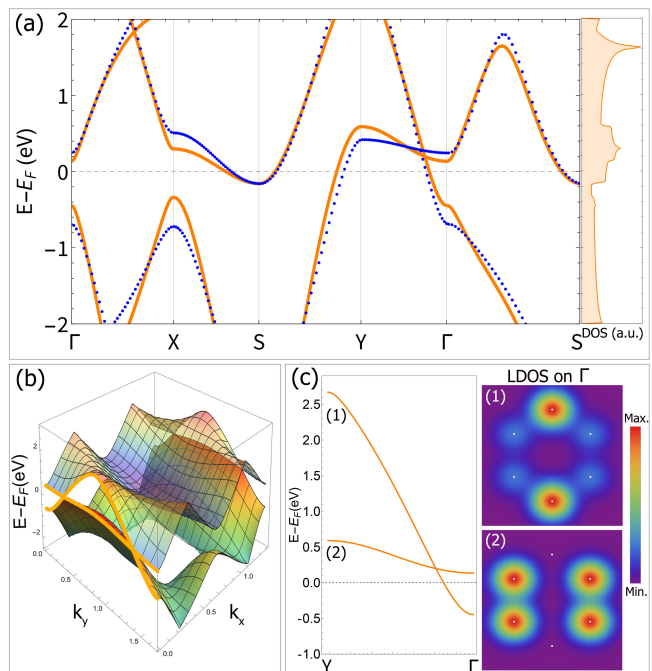


FIG. 2. (a) Biphenylene electronic structure: DFT calculations (blue dotted curves) and TB results (orange bands) considering onsite energy $\epsilon = -1.7 \text{ eV}$, in-plane first neighbors hopping $t_1 = -3.3 \text{ eV}$ and hopping range parameter $\beta = 2.2$. The DOS corresponding to the TB bands is plotted at the right side of the panel. (b) 2D tight-binding biphenylene energy bands, showing the type-II Dirac cone in orange. (c) Zoom of the band structure along the $Y - \Gamma$ high-symmetry line focusing on the type-II Dirac cone. At the right of the panel, the LDOS for the two bands forming the Dirac cone is depicted. The position of the atoms inside the unit cell are marked with white dots. Red and purple corresponds to the maximum and minimum probability density, respectively.

A zoom of the bands along $Y - \Gamma$ constituting the type-II Dirac cone, labeled (1) and (2), is presented in Fig. 2(c). The local density of states (LDOS) of the respective bands, calculated at the Y-point, are depicted at the side of the electronic bands. The max LDOS values are complementary in space, i.e., they are localized in different regions of the unit cell. At the crossing energy

TABLE I. Lattice parameters for the monolayer obtained from DFT (PBE-GGA) relaxation and fitted parameters for the TB calculations.

Lattice Parameters	2D TB Parameters
$d_1 = 1.42 \text{ \AA}$	$t_1 = -3.3 \text{ eV}$
$d_2 = 1.44 \text{ \AA}$	$t_0 = -0.33 \text{ eV}$
$d_3 = 1.50 \text{ \AA}$	$\alpha = 5.0$
$d_4 = 1.47 \text{ \AA}$	$\beta = 2.2$

(not shown here), all sites have a nonzero density. It is important to emphasize that the use of a tight-binding parametrization incorporating an exponential decay is crucial in our model to obtain the predicted type-II Dirac cone in biphenylene and similar materials, in agreement with DFT calculations.

The overall picture of the hopping decay parametrization with the neighbor distances is shown in Fig. 3, with the hopping scheme in the inset, where each group of neighbors is highlighted with colored regions, I, II, and III. Region I corresponds to hoppings between atoms with primary bonds (black solid lines), region II is for intermediate distances (colored solid lines) and region III corresponds to long-range hoppings (colored dashed lines). The slope of the bands is determined by the β parameter

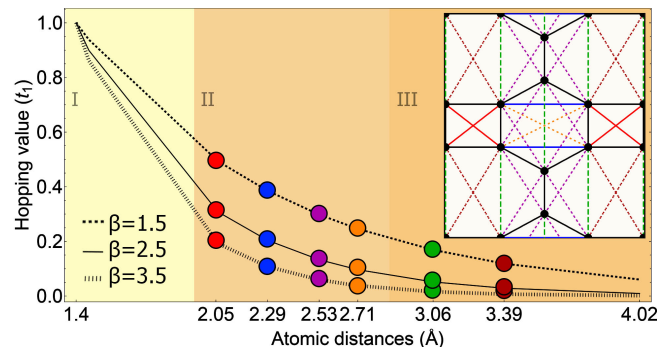


FIG. 3. Illustration of in-plane hopping energies as a function of the atomic lattice distances for different values of the decay parameter β . Colored circles illustrate hoppings at different lattice distances, matching the color code employed in the schematic lattice geometry shown in the inset. The distances/hoppings are grouped by shaded regions, I, II, and III, respectively.

ter, and altering it affects carrier velocities. This adjustment can be tuned to achieve the desired characteristics of the bands. Additionally, it is essential to take into account a sufficient number of neighbors. To achieve the desired type-II Dirac cone we must include hoppings up to region III, which is equivalent to consider distances greater than those marked by green dashed lines ($> 3 \text{ \AA}$) in the schematic inset. Not considering enough hopping parameters results in a completely flat energy band along the $Y - \Gamma$ direction in one of the branches of the Dirac cone, changing its character to type-III [32, 37]. Therefore, a careful choice of both the β parameter, and

hence the range of neighbors included, is critical to obtain the desired band features. We consider that this parametrization approach will also be helpful in other systems, where intricate symmetries and numerous hopping distances may hinder the derivation of optimal physical parameters for theories based in a TB model theory of the structure.

B. Bilayer biphenylene

For bilayer biphenylene systems, we have included the van der Waals interaction in the DFT calculations with a vdW-DF2 functional. As in the case of the monolayer, the lattice parameters included in TB calculations were obtained from previous DFT relaxations. We find that the intralayer and the internal angles are the same as for the monolayer.

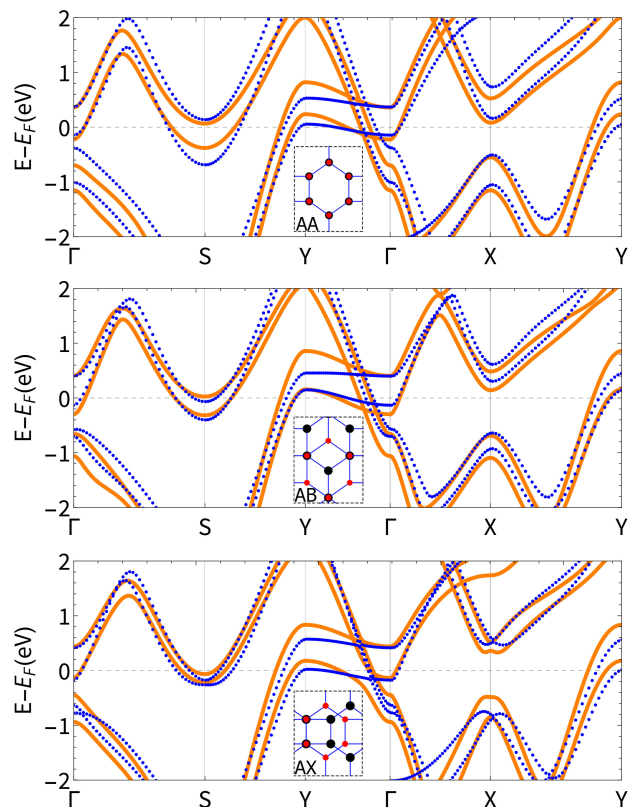


FIG. 4. Bilayer biphenylene band structures for the three stackings considered: (a) AA, (b) AB, and (c) AX stackings. The corresponding unit cells are shown in the insets, marked with dashed lines. DFT bands are shown with blue dots, and TB as orange curves; the parameters chosen are $\alpha = 5.0$, $\beta = 2.2$, $t_0 = -0.33 \text{ eV}$, $t_1 = -3.3 \text{ eV}$, $\epsilon = -1.7 \text{ eV}$.

Table II displays the averaged interlayer d_{\perp} distances, since from DFT relaxation slight differences are seen in the z -coordinates. Previous DFT calculations [38] predicted a biphenylene interlayer distance of 3.36 \AA in AA stacking, a value notably close to that of bilayer graphene

TABLE II. Bilayer lattice parameters obtained from the DFT relaxed structures within vdW-DF2.

Stackings	Mean d_{\perp}	a_1^{-}	a_2^{-}
AA	3.51 Å	3.83839 Å	4.53791 Å
AB	3.39 Å	3.83767 Å	4.53921 Å
AX	3.43 Å	3.83637 Å	4.53844 Å

(3.42 Å). However, our calculations yield a larger distance for the AA stacking. The values for the three studied stackings reveal a small variation for the interlayer distances, as summarized in Table II. In our calculation, the AB stacking has the smallest interlayer spacing.

In Fig. 4 we compare the DFT and TB band structures of the three stacking configurations, AA, AB and AX. We verify that the agreement between TB and DFT bands is very satisfactory. Notice that, due to interlayer coupling, the type-II Dirac cones are doubled, as expected. Moreover, one of the cones is now at the Fermi energy for the three proposed stackings. The TB fits correspond to $\alpha = 5.0$ and $t_0 = -0.33$ eV for the interlayer coupling; the same intralayer parameters used in the case of the monolayer are adopted. Additionally, we have performed calculations for the bilayers with the three functionals GGA-PBE, vdW-DF, and vdW-DF2, to compare the total energies of the three stackings. All packings were found to be stable and had comparable total energies. The smallest interlayer distances correspond to the vdW-DF2 functional. In the supplemental material we show a comparison of the energy bands computed using the different DFT functionals.

IV. ARMCHAIR NANORIBBONS

In what follows, we perform biphenylene nanoribbon (NR) calculations to exemplify the effectiveness of the proposed parametrization in such quasi-1D systems. The coordinates are obtained from the relaxed GGA-PBE DFT calculations done for the 2D monolayer. We have verified by comparison to other DFT calculations [20] that edge effects are not important, so by repeating the monolayer relaxed unit cell we obtain those of the nanoribbons employed in the TB calculations. We focus on the armchair edges, which are known to have semiconductor nature for smaller widths. We have found that the optimal parametrization has the same in-plane hopping $t_1 = 3.3$ eV used for the 2D system, and an adjusted on-site energy ϵ and exponential parameter β ; $\epsilon = -1.3$ eV and $\beta = 2.6$, respectively. These modifications are necessary to better describe confined states in quasi-1D periodic systems, in contrast to relaxed DFT nanoribbons from previous energy band results [20].

A type-II Dirac cone is also observed for nanoribbons with an odd number of hexagons inside the unit cell across their width. A gap opens, destroying the cone, for those with an even width, as highlighted in Fig. 5(a)

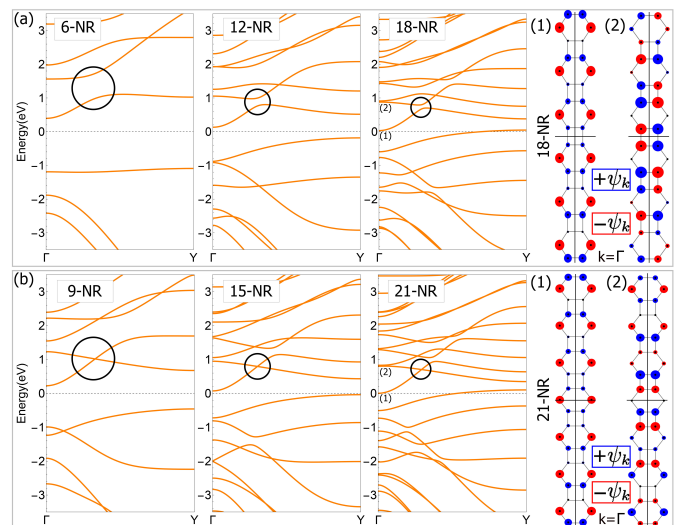


FIG. 5. Electronic band structures of armchair nanoribbons with (a) even (6-NR, 12-NR, and 18-NR) and (b) odd (9-NR, 15-NR, and 21-NR) number of sites along the width. Wavefunction $\psi_{k=\Gamma}$ values and signs for the 18-NR and 21-NR, represented by the sizes and colors of circles within the unit cell, respectively, for bands (1) and (2).

and (b) by black circles at the anticrossing or crossing regions, for even and odd ribbons, respectively. The projected wavefunctions inside the unit cells at Γ point, for the 18-NR and 21-NR, are depicted at the right side of the respective band structures. The sign of the wavefunction is represented by red and blue and their amplitudes by the disk sizes. Notice that the wavefunctions of the low-lying band at Γ , labeled (1), presents two mirror symmetries with respect to the horizontal (M_h) and vertical (M_v) planes marked with black lines, as well as inversion symmetry (I). However, the wavefunction of the the upper band, labeled (2), has fewer (and) different symmetries, which vary with the nanoribbon width. In the case shown in Fig. 5(a), the 18-NR, it is M_h ; for Fig. 5(b), corresponding to 21-NR, it is M_v . The horizontal mirror symmetry is important for the confined wavefunctions; note that the probability density is symmetric with respect to the longitudinal axes of the ribbons. Therefore, if the wavefunctions of bands (1) and (2) share this symmetry (for even widths), their bands anticross, whereas for odd ribbons, for which these bands do not share this reflection symmetry, the bands cross and the Dirac cone is preserved. Similar symmetry arguments have successfully explained even-odd effects in other graphene-based nanoribbons [47] and slabs of topological materials [48, 49].

The same parametrization was also employed for the study of wide ribbons. In Fig. 6(a) we present three edge configurations in the armchair features: symmetric closed hexagons (SCH), anti-symmetric (AS), and symmetric open hexagons (SOH), represented by blue, red, and green edges, respectively. Using the same color

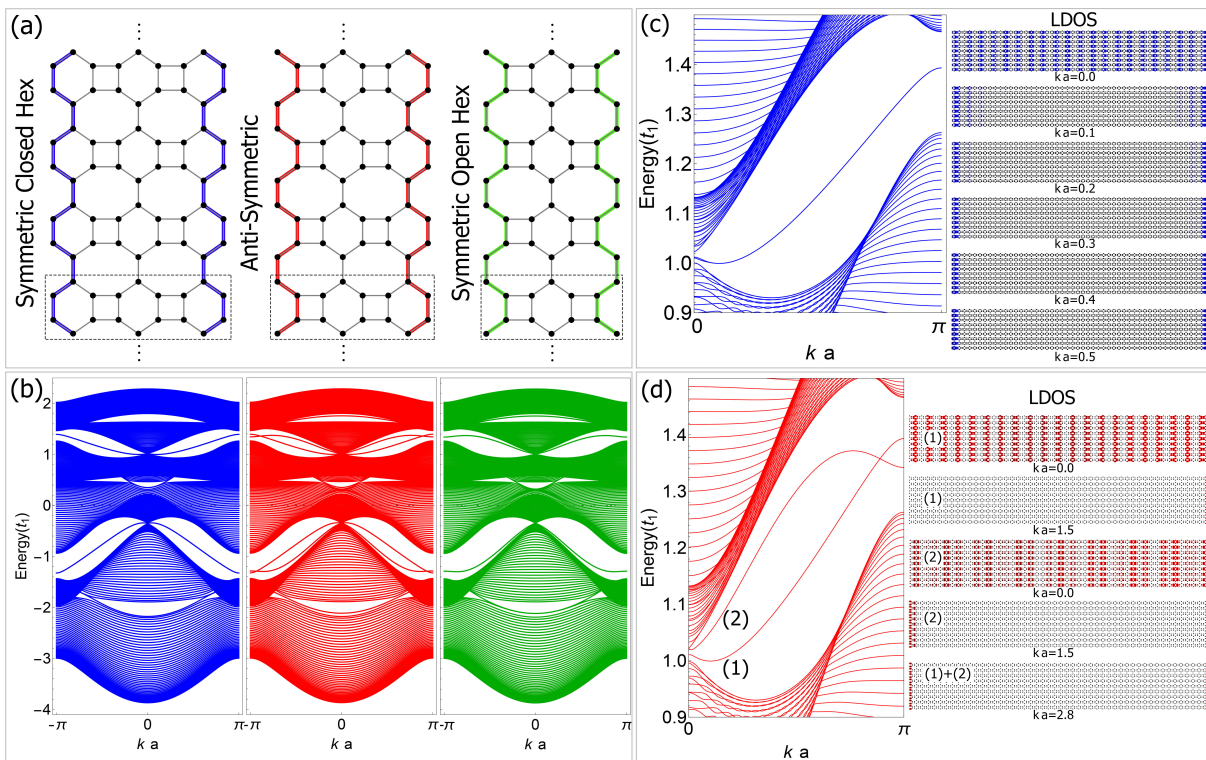


FIG. 6. (a) 9-NR Armchair nanoribbons geometries for three edge configurations in blue, red and green, respectively: symmetric closed hexagons, anti-symmetric, and symmetric open hexagons. (b) Electronic bands of 50-NRs for the three edge configurations ($\beta = 2.6$ and $\epsilon = 0$). Zoom of the electronic bands of the (c) SCH and (d) AS 50-NRs and projected LDOS for different ka values over the nanoribbon sites highlighted in black in panel (a).

scheme, the electronic bands for each edge configuration are shown at Fig. 6(b) in terms of t_1 . The average energy states are the same, changing only for the isolated states localized between the bulk energy bands for each one of the three edge symmetries, verified as emergent topological features in biphenylene systems [37]. A zoom in the two-fold degenerate SCH band structure (blue curves) is shown in Fig. 6(c). The LDOS is computed for this specific state between $k = 0$ and $k = 0.5$. At $k = 0$, we note that the charge density is spread over all the nanoribbon when the edge bands meet the bulk bands. A transition in the charge distribution happens, however, as shown for $ka = 0.1$ up to $ka = 0.5$, at the Brillouin zone boundary. Highly localized states at the nanoribbon edges for $k \neq 0$ emerge.

V. CONCLUSIONS

In summary, we have derived a robust TB parametrization based in DFT calculations that successfully describes the electronic structure of a variety of biphenylene systems comprising monolayers, bilayers and nanoribbons of diverse width. We have verified the presence of a type-II Dirac cone in both monolayer and bilayer geometries, in agreement with previous works. The DFT and tight-binding integration via the relaxed structures obtained

from first-principles calculations, made possible to create a realistic spatial distribution for the TB model, which allows us to accurately describe the electronic properties of biphenylene. An exponential decaying hopping evaluation in TB successfully yields the expected band structures, in agreement with DFT calculations. In fact, our TB parametrization also encapsulates essential symmetries inherent to such structures, and extending the number of hoppings up to third neighboring distances ensures that this Dirac cone is of type II instead of type III. We therefore suggest that such an exponential hopping decay can be essential for properly describing similar intricate carbon-based systems with hybrid geometric symmetries, such as pentagraphene and graphyne.

We have also presented two novel bilayer symmetric stackings, AB and AX, not studied so far, and described them within the same technique. Due to interlayer coupling, one of the Dirac cones is at the Fermi energy; this characteristic may reveal novel transport properties for these systems. Moreover, we expect these new stackings to be of a similar stability to the already investigated AA biphenylene, making them experimentally feasible.

Using this joint approach, we have been able to characterize not only the type-II Dirac cone present in the monolayer and bilayer stackings, but also their 1D counterparts, showing an even-odd effect in the Dirac cone of biphenylene nanoribbons that we relate to the sym-

metry of the corresponding wavefunctions. These features were distinguished in the electronic bands, by crossing and anti-crossing cones at the same energy range as the 2D systems. Besides this accurate description of small nanoribbons, we have extended our approach to nanoribbons of bigger width, which are successfully described within our formalism. The analysis of different symmetric and anti-symmetric edges for these wider nanoribbons reveals a set of robust isolated states, localized between bulk energy bands, where we have verified a two fold degeneracy. By projecting the charge over the real space within symmetric edged-nanoribbons we verify that those states are in fact localized at the extremes of such structures, being classified as edge states in agreement with previous works including only first neighbors [37], predicting them to be topological. Furthermore, at anti-symmetric edges, the isolated band degeneracy is split into two singular bands, which are responsible for the charge distribution at opposite edge sites over the nanoribbons. Edge states are found to be sensitive to the symmetry details of the unit cell borders. Our approach provides a global framework to characterize and analyze the behavior of the type-II Dirac cone within 1D and 2D biphenylene structures, and successfully comprises im-

portant symmetries inherent in such carbon-based materials. We have presented unreported bilayer stackings, as well as diverse nanoribbon configurations, and expect our findings to motivate further theoretical and experimental research.

ACKNOWLEDGMENTS

The authors would like to thank the INCT de Nanomateriais de Carbono for providing support on the computational infrastructure. LLL thanks the CNPq scholarship. AL thanks the CNPq and FAPERJ under grants E-26/202.567/2019 and E-26/200.569/2023. LC and OAG acknowledge financial support from the Agencia Estatal de Investigación of Spain under grant PID2022-136285NB-C31, and from grant (MAD2D-CM)- (UCM5), Recovery, Transformation and Resilience Plan, funded by the European Union - NextGenerationEU. OAG acknowledges the support of grant PRE2019-088874 funded by MCIN/AEI/10.13039/501100011033 and by “ESF Investing in your future”.

-
- [1] K. S. Novoselov, A. K. Geim, S. V. Morozov, D. Jiang, Y. Zhang, S. V. Dubonos, I. V. Grigorieva, A. A. Firsov, Electric field effect in atomically thin carbon films, *Science* 306 (2004) 666–669. doi:10.1126/science.1102896.
- [2] K. S. Novoselov, D. Jiang, F. Schedin, T. J. Booth, V. V. Khotkevich, S. V. Morozov, A. K. Geim, Two-dimensional atomic crystals, *Proceedings of the National Academy of Sciences* 102 (2005) 10451–10453. doi:10.1073/pnas.0502848102.
- [3] M. Xu, T. Liang, M. Shi, H. Chen, Graphene-like two-dimensional materials, *Chem. Rev.* 113 (5) (2013) 3766–3798. doi:10.1021/cr300263a. URL <https://doi.org/10.1021/cr300263a>
- [4] A. K. Geim, I. V. Grigorieva, Van der waals heterostructures, *Nature* 499 (7459) (2013) 419–425. doi:10.1038/nature12385. URL <https://doi.org/10.1038/nature12385>
- [5] P. Miró, M. Audiffred, T. Heine, An atlas of two-dimensional materials, *Chem. Soc. Rev.* 43 (18) (2014) 6537–6554. doi:10.1039/C4CS00102H. URL <http://xlink.rsc.org/?DOI=C4CS00102H>
- [6] M. Ashton, J. Paul, S. B. Sinnott, R. G. Hennig, Topology-scaling identification of layered solids and stable exfoliated 2d materials, *Phys. Rev. Lett.* 118 (2017) 106101. doi:10.1103/PhysRevLett.118.106101. URL <https://link.aps.org/doi/10.1103/PhysRevLett.118.106101>
- [7] S. Haastrop, M. Strange, M. Pandey, T. Deilmann, P. S. Schmidt, N. F. Hinsche, M. N. Gjerding, D. Torelli, P. M. Larsen, A. C. Riis-Jensen, J. Gath, K. W. Jacobsen, J. J. Mortensen, T. Olsen, K. S. Thygesen, The Computational 2D Materials Database: high-throughput modeling and discovery of atomically thin crystals, *2D Materials* 5 (4) (2018) 042002. doi:10.1088/2053-1583/aacfc1. URL <https://iopscience.iop.org/article/10.1088/2053-1583/aacfc1/meta>
- [8] H. Lu, S.-D. Li, Two-dimensional carbon allotropes from graphene to graphyne, *J. Mater. Chem. C* 1 (2013) 3677–3680. doi:10.1039/C3TC30302K. URL <http://dx.doi.org/10.1039/C3TC30302K>
- [9] Y. Hu, C. Wu, Q. Pan, et al., Synthesis of gamma-graphyne using dynamic covalent chemistry, *Nat. Synth* 1 (2022) 449–454. doi:10.1038/s44160-022-00068-7. URL <https://doi.org/10.1038/s44160-022-00068-7>
- [10] Artificial carbon allotrope gamma-graphyne: Synthesis, properties, and applications, *Giant* 13 (2023) 100140. doi:<https://doi.org/10.1016/j.giant.2023.100140>.
- [11] D. C. M. Rodrigues, L. L. Lage, P. Venezuela, A. Latgé, Exploring the enhancement of the thermoelectric properties of bilayer graphyne nanoribbons, *Phys. Chem. Chem. Phys.* 24 (2022) 9324–9332. doi:10.1039/D1CP05491K. URL <http://dx.doi.org/10.1039/D1CP05491K>
- [12] D. C. M. Rodrigues, R. G. Amorim, A. Latgé, P. Venezuela, Improving the sensitivity of graphyne nanosensor by transition metal doping, *Carbon* 212 (2023) 118087. doi:[doi:10.1016/j.carbon.2023.118087](https://doi.org/10.1016/j.carbon.2023.118087).
- [13] X. Zheng, S. Chen, J. Li, H. Wu, C. Zhang, D. Zhang, X. Chen, Y. Gao, F. He, L. Hui, H. Liu, T. Jiu, N. Wang, G. Li, J. Xu, Y. Xue, C. Huang, C. Chen, Y. Guo, T.-B. Lu, D. Wang, L. Mao, J. Zhang, Y. Zhang, L. Chi, W. Guo, X.-H. Bu, H. Zhang, L. Dai, Y. Zhao, Y. Li, Two-dimensional carbon graphdiyne: Advances in fundamental and application research, *ACS Nano* 17 (15) (2023) 14309–14346. doi:10.1021/acsnano.3c03849.

- URL <https://doi.org/10.1021/acsnano.3c03849>
- [14] V. H. Crespi, L. X. Benedict, M. L. Cohen, S. G. Louie, Prediction of a pure-carbon planar covalent metal, *Phys. Rev. B* 53 (1996) R13303–R13305. doi:10.1103/PhysRevB.53.R13303.
URL <https://link.aps.org/doi/10.1103/PhysRevB.53.R13303>
- [15] J. Nisar, X. Jiang, B. Pathak, J. Zhao, T. W. Kang, R. Ahuja, Semiconducting allotrope of graphene, *Nanotechnology* 23 (38) (2012) 385704. doi:10.1088/0957-4484/23/38/385704.
- [16] C.-P. Tang, S.-J. Xiong, W.-J. Shi, J. Cao, Two-dimensional pentagonal crystals and possible spin-polarized dirac dispersion relations, *Jour. of Appl. Phys.* 115 (11) (2014) 113702. doi:10.1063/1.4868679.
- [17] S. Zhang, J. Zhou, Q. Wang, X. Chen, Y. Kawazoe, P. Jena, Penta-graphene: A new carbon allotrope, *Proceedings of the National Academy of Sciences* 112 (8) (2015) 2372–2377. doi:10.1073/pnas.1416591112.
- [18] L.-C. Xu, R.-Z. Wang, M.-S. Miao, X.-L. Wei, Y.-P. Chen, H. Yan, W.-M. Lau, L.-M. Liu, Y.-M. Ma, Two dimensional dirac carbon allotropes from graphene, *Nanoscale* 6 (2014) 1113–1118. doi:10.1039/C3NR04463G.
- [19] A. Bandyopadhyay, S. Datta, D. Jana, et al., The topology and robustness of two dirac cones in s-graphene: A tight binding approach, *Scientific Reports* 10 (2020) 2502. doi:10.1038/s41598-020-59262-2.
- [20] Q. Fan, L. Yan, M. Tripp, O. Krejčí, S. Dimosthenous, S. Kachel, M. Chen, A. Foster, U. Koert, P. Liljeroth, J. Gottfried, Biphenylene network: A nonbenzenoid carbon allotrope, *Science* 372 (6544) (2021) 852–856. doi:10.1126/science.abg4509.
- [21] E. C. A. T. Balaban, C. C. Rentia, *Rev. Roum. Chim.* 13 (1968) 231–247.
- [22] M. A. Hudspeth, B. W. Whitman, V. Barone, J. E. Peralta, Electronic properties of the biphenylene sheet and its one-dimensional derivatives, *ACS Nano* 4 (8) (2010) 4565–4570. doi:10.1021/nn100758h.
- [23] Y. Luo, C. Ren, Y. Xu, J. Yu, S. Wang, M. Sun, A first principles investigation on the structural, mechanical, electronic, and catalytic properties of biphenylene, *Scientific Reports* 11 (2021) 98589. doi:10.1038/s41598-021-98589-4.
- [24] K. Ke, K. Meng, J. Rong, X. Yu, Biphenylene: A two-dimensional graphene-based coating with superior anti-corrosion performance, *Materials* 15 (16) (2022) 5675. doi:10.3390/ma15165675.
URL <https://doi.org/10.3390/ma15165675>
- [25] S. Demirci, T. Gorkan, S. Çallıoğlu, V. O. Özçelik, J. V. Barth, E. Aktürk, S. Çiraci, Hydrogenated carbon monolayer in biphenylene network offers a potential paradigm for nanoelectronic devices, *The Journal of Physical Chemistry C* 126 (36) (2022) 15491–15500. doi:10.1021/acs.jpcc.2c04453.
URL <https://doi.org/10.1021/acs.jpcc.2c04453>
- [26] Y.-W. Son, H. Jin, S. Kim, Magnetic ordering, anomalous lifshitz transition, and topological grain boundaries in two-dimensional biphenylene network, *Nano Lett.* 22 (2022) 3112. doi:10.1021/acs.nanolett.2c00528.
- [27] P.-F. Liu, J. Li, C. Zhang, X. H. Tu, J. Zhang, P. Zhang, B.-T. Wang, D. J. Singh, Type-ii dirac cones and electron-phonon interaction in monolayer biphenylene from first-principles calculations, *Phys. Rev. B* 104 (2021) 235422. doi:10.1103/PhysRevB.104.235422.
- [28] I. Alcón, G. Calogero, N. Papior, A. Antidormi, K. Song, A. W. Cummings, M. Brandbyge, S. Roche, Unveiling the multiradical character of the biphenylene network and its anisotropic charge transport, *Journal of the American Chemical Society* 144 (18) (2022) 8278–8285. doi:10.1021/jacs.2c02178.
- [29] A. Bafekry, M. Faraji, M. M. Fadlallah, H. R. Jappor, S. Karbasizadeh, M. Ghergherehchi, D. Gogova, Biphenylene monolayer as a two-dimensional nonbenzenoid carbon allotrope: a first-principles study, *Jour. of Phys.: Cond. Matt.* 34 (1) (2022) 015001. doi:10.1088/1361-648X/ac2a7b.
- [30] Y. Hou, K. Ren, Y. Wei, D. Yang, Z. Cui, K. Wang, Opening a band gap in biphenylene monolayer via strain: A first-principles study, *Molecules* 28 (10) (2023) 4178. doi:10.3390/molecules28104178.
URL <https://doi.org/10.3390/molecules28104178>
- [31] S. Lee, A. Singh, H. Lee, Band gap engineering of 2d biphenylene carbon sheets with hydrogenation, *J. Korean Phys. Soc.* 79 (2021) 846–850. doi:10.1007/s40042-021-00312-x.
URL <https://doi.org/10.1007/s40042-021-00312-x>
- [32] S. Mo, J. Seo, S. K. Son, S. Kim, J. N. Rhim, H. Lee, Engineering two-dimensional nodal semimetals in functionalized biphenylene by fluorine adatoms, *arXiv:2401.17607* doi:10.48550/arXiv.2401.17607.
- [33] K. Ke, M. K., J. Rong, X. Yu, Biphenylene: A two-dimensional graphene-based coating with superior anti-corrosion performance, *Materials* 15 (2022) 5675. doi:10.3390/ma15165675.
- [34] A. Kumar, P. Senapati, P. Parida, Theoretical insights into the structural, electronic and thermoelectric properties of the inorganic biphenylene monolayer, *Phys. Chem. Chem. Phys.* 26 (2024) 2044–2057. doi:10.1039/D3CP03088A.
- [35] Z.-X. Xie, X.-K. Chen, X. Yu, Y.-X. Deng, Y. Zhang, W.-X. Zhou, P.-Z. Jia, Intrinsic thermoelectric properties in biphenylene nanoribbons and effect of lattice defects, *Computational Materials Science* 220 (2023) 112041. doi:10.1016/j.commatsci.2022.112041.
- [36] O. Farzadian, M. Zarghami Dehaghani, K. V. Kostas, A. H. Mashhadzadeh, C. Spitas, A theoretical insight into phonon heat transport in graphene/biphenylene superlattice nanoribbons: a molecular dynamic study, *Nanotechnology* 33 (35) (2022) 355705. doi:10.1088/1361-6528/ac733e.
- [37] K. Koizumi, H. T. Phan, K. Nishigomi, K. Wakabayashi, *Phys. Rev. B* 109 (2024) 035431. doi:10.1103/PhysRevB.109035431.
- [38] S. Chowdhury, S. Ghosal, D. Mondal, D. Jana, First-principles and machine-learning study of electronic and phonon transport in carbon-based aa-stacked bilayer biphenylene nanosheets, *Journal of Physics & Chemistry of Solids* 170 (2022) 110909. doi:10.1016/j.jpccs.2022.110909.
URL <https://doi.org/10.1016/j.jpccs.2022.110909>
- [39] G. Li, A. Luican, J. M. B. Lopes dos Santos, A. H. Castro Neto, A. Reina, J. Kong, E. Y. Andrei, Observation of van hove singularities in twisted graphene layers, *Nature Physics* 6 (2) (2010) 109–113. doi:10.1038/nphys1463.
- [40] E. S. Morell, P. Vargas, L. Chico, L. Brey, Charge redistribution and interlayer coupling in twisted bilayer graphene under electric fields, *Phys. Rev. B* 84 (2011)

195421. doi:10.1103/PhysRevB.84.195421.
- [41] J. M. Soler, E. Artacho, J. D. Gale, A. García, J. Junquera, P. Ordejón, D. Sánchez-Portal, The siesta method for ab initio order-n materials simulation, *Jour. of Phys.: Cond. Matt.* 14 (11) (2002) 2745. doi:10.1088/0953-8984/14/11/302.
- [42] A. García, N. Papior, A. Akhtar, E. Artacho, V. Blum, E. Bosoni, P. Brandimarte, M. Brandbyge, J. I. Cerdá, F. Corsetti, R. Cuadrado, V. Dikan, J. Ferrer, J. Gale, P. García-Fernández, V. M. García-Suárez, S. García, G. Huhs, S. Illera, R. Korytár, P. Koval, I. Lebedeva, L. Lin, P. López-Tarifa, S. G. Mayo, S. Mohr, P. Ordejón, A. Postnikov, Y. Pouillon, M. Pruneda, R. Robles, D. Sánchez-Portal, J. M. Soler, R. Ullah, V. W.-z. Yu, J. Junquera, Recent developments and applications, *The Journal of Chemical Physics* 152 (2020) 204108. doi:10.1063/5.0005077.
- [43] J. P. Perdew, K. Burke, M. Ernzerhof, Generalized gradient approximation made simple, *Phys. Rev. Lett.* 77 (1996) 3865–3868. doi:10.1103/PhysRevLett.77.3865. URL <https://link.aps.org/doi/10.1103/PhysRevLett.77.3865>
- [44] M. Dion, H. Rydberg, E. Schröder, D. C. Langreth, B. I. Lundqvist, Van der waals density functional for general geometries, *Phys. Rev. Lett.* 92 (2004) 246401. doi:10.1103/PhysRevLett.92.246401. URL <https://link.aps.org/doi/10.1103/PhysRevLett.92.246401>
- [45] G. Román-Pérez, J. M. Soler, Efficient implementation of a van der waals density functional: Application to double-wall carbon nanotubes, *Phys. Rev. Lett.* 103 (2009) 096102. doi:10.1103/PhysRevLett.103.096102. URL <https://link.aps.org/doi/10.1103/PhysRevLett.103.096102>
- [46] K. Lee, E. D. Murray, L. Kong, B. I. Lundqvist, D. C. Langreth, Higher-accuracy van der waals density functional, *Phys. Rev. B* 82 (2010) 081101. doi:10.1103/PhysRevB.82.081101. URL <https://link.aps.org/doi/10.1103/PhysRevB.82.081101>
- [47] K. Čerņevičs, M. Pizzochero, O. V. Yazyev, Even-odd conductance effect in graphene nanoribbons induced by edge functionalization with aromatic molecules: basis for novel chemosensors, *The European Physical Journal Plus* 135 (8) (Aug. 2020). doi:10.1140/epjp/s13360-020-00696-y. URL <http://dx.doi.org/10.1140/epjp/s13360-020-00696-y>
- [48] A. L. Araújo, G. J. Ferreira, T. M. Schmidt, Suppressed topological phase transitions due to nonsymmorphism in snite stacking, *Scientific Reports* 8 (1) (Jun. 2018). doi:10.1038/s41598-018-27827-x. URL <http://dx.doi.org/10.1038/s41598-018-27827-x>
- [49] O. Arroyo-Gascón, Y. Baba, J. I. Cerdá, O. de Abril, R. Martínez, F. Domínguez-Adame, L. Chico, Persistence of symmetry-protected dirac points at the surface of the topological crystalline insulator snite upon impurity doping, *Nanoscale* 14 (19) (2022) 7151–7162. doi:10.1039/d1nr07120c. URL <http://dx.doi.org/10.1039/d1nr07120c>